CORE
Metadata, citation and similar papers at core.ac.uk
Provided by Elsevier - Publisher Connector

International Journal of Solids and Structures 50 (2013) 996–1004

Contents lists available at SciVerse ScienceDirect

International Journal of Solids and Structures

journal homepage: www.elsevier.com/locate/ijsolstr

Elasticity of anti-tetrachiral anisotropic lattices

Y.J. Chen [a,b], F. Scarpa [b,*], Y.J. Liu [c], J.S. Leng [a,*]

[a] Centre for Composite Materials and Structures, No. 2 YiKuang Street, Science Park of Harbin Institute of Technology (HIT), P.O. Box 3011, Harbin 150080, China
[b] Advanced Composites Centre for Innovation and Science, University of Bristol, Bristol BS8 1TR, UK
[c] Department of Aerospace Science and Mechanics, No. 92 West Dazhi Street, Harbin Institute of Technology (HIT), P.O. Box 301, Harbin, PR China

ARTICLE INFO

Article history:
Received 11 June 2012
Received in revised form 26 October 2012
Available online 21 December 2012

Keywords:
Anti-tetrachiral lattices
Anisotropic
Negative Poisson's ratio
Finite element method (FEM)
Elastic constants

ABSTRACT

This work describes the theoretical, numerical and experimental in-plane and out-of-plane elastic behavior of a class of anti-tetrachiral lattice structures with in-plane negative Poisson's ratios and anisotropic behavior. Closed form analytical solutions related to the uniaxial stiffness, in-plane Poisson's ratio and bounds for the transverse shear modulus are derived, and compared against homogenization-based finite element methods and experimental tests performed on rapid prototyping-made samples. The benchmarked models are then used to investigate the behaviors of the anisotropic negative Poisson's ratio structures against the geometry parameters defining the unit cell. The results show the existence of large variations in linear elastic constants and degree of anisotropy, which can be achieved by changing the lattice geometry parameters. The analysis presented in this work provides meaningful guidance to assist design anti-tetrachiral anisotropic lattices, which could serve as sandwich panel cores in aerospace applications.

© 2012 Elsevier Ltd. All rights reserved.

1. Introduction

Cellular and lattice structures have attracted the attention of many researchers around the world for several decades, due to their significant lightweight and out-of-plane stiffness properties (Bitzer, 1997). A primary application for cellular solids is their use as sandwich core materials in a variety of engineering technologies, such as marine, aerospace and automotive lightweight structures (Alderson et al., 2010a,b). The conventional hexagonal honeycomb is a typical example of cellular core configuration, with unit cells made of ribs with equal length and an internal cell angle of $\pi/6$ (Gibson and Ashby, 1997). Over-expanded centresymmetric honeycomb configurations with special orthotropic properties can also be developed when varying the cell wall aspect ratio and internal cell angle, always with positive values (Bezazi et al., 2005; Gibson and Ashby, 1997). Hexagonal honeycombs with convex configuration (i.e. positive internal cell angle) exhibit anticlastic or saddle-shape curvatures when subject to out-of-plane bending (Evans, 1991; Lakes, 1987; Masters and Evans, 1996), making more problematic the use of classical cores in sandwich structures with complex geometry (Evans and Alderson, 2000b). On the opposite, negative Poisson's ratio (auxetic) solids feature synclastic curvature behaviors, making possible therefore to produce dome-shaped surfaces when bent out-of-plane (Evans and Alderson, 2000a; Lakes, 1987). Auxetic cellular structures have also been used to prototype morphing wings (Bettini et al., 2010; Martin et al., 2008; Spadoni et al., 2006), radomes (Scarpa et al., 2003), adaptive and deployable structures (Hassan et al., 2008).

An attractive auxetic honeycomb structure is the structural chiral configuration (Prall and Lakes, 1996). Structural chiral honeycombs are composed by nodes connected by tangent ligaments, providing an in-plane negative Poisson's ratio effect due to the bending-dominated deformation of the connecting ribs to the rotating nodes. Apart from the synclastic curvatures feature common to auxetic honeycombs (Evans and Alderson, 2000b), the chiral honeycombs provide the advantages to partially decouple the transverse shear and flatwise compressive strengths, which are enhanced by ligaments and nodes, respectively (Scarpa et al., 2007; Spadoni et al., 2005). Therefore, the through-thickness mechanical performance could be improved through the selection of special geometry parameters related to the nodes and ligaments (Alderson et al., 2010b; Gaspar et al., 2005; Scarpa et al., 2007). Chiral honeycombs possess 3, 4 and 6 ligaments (trichiral, tetrachiral and hexachiral). It is also possible to connect the same side of the ligaments to the adjacent nodes, obtaining therefore anti-trichiral, anti-tetrachiral and anti-hexachiral honeycombs, respectively (Grima, 2000). The chiral honeycomb with a theoretical in-plane Poisson's ratio of -1 was first reported by Prall and Lakes (1996), while a large class of structural chiral topologies has been evaluated analytically by Grima (2000). Alderson et al. (2010a) examined the in-plane linear elastic properties of chiral honeycomb

* Corresponding authors. Tel.: +86 (0) 451 86402328; fax: +86 (0) 451 86402328 (J.S. Leng), tel.: +44 (0) 1173315306; fax: +44 (0) 1179272771 (F. Scarpa).
E-mail addresses: f.scarpa@bris.ac.uk, f.scarpa@bristol.ac.uk (F. Scarpa), lengjs@hit.edu.cn (J.S. Leng).

0020-7683/$ - see front matter © 2012 Elsevier Ltd. All rights reserved.
http://dx.doi.org/10.1016/j.ijsolstr.2012.12.004

attached with 3, 4 and 6 ligaments. The transverse elastic properties of these chiral honeycombs were further investigated by Lorato et al. (2010). Isotropic anti-tetrachiral configurations show on average in-plane stiffness one order of magnitude higher compared to trichiral configurations for the same relative wall thickness ratio, although the deformation mechanism of the ligament under compression (half-wave) provides an equivalent in-plane compressive modulus lower than the classical tetrachiral configuration (Alderson et al., 2010a). The transverse shear modulus of isotropic anti-tetrachiral lattices is similar to the one of 3-ligaments configurations, and 50% lower on average compared to hexachiral configurations (Lorato et al., 2010). However, the normalized flatwise compression behavior of isotropic anti-tetrachiral configurations is equivalent to the one of 6-ligaments hexagonal chiral topologies (Miller et al., 2010). Moreover, the anti-tetrachiral configuration shows a stable in-plane negative Poisson's ratio (~−1 (Alderson et al., 2010a)), and it is not subjected to global coupling of uniaxial compression and in-plane rotation of the specimen when loaded, making it therefore a structure exhibiting a more uniform deformation behavior under the application of external forces. One aspect that has not been considered in open literature- to the best of the Author's knowledge- is the mechanical behavior of anisotropic architectures related to chiral structures. Since the anti-tetrachiral honeycomb exhibits a considerable potential for engineering application, such as structural health monitoring (Jenal et al., October 20–22, 2009) and aerospace components (Miller et al., 2010), it is interesting to study its anisotropic properties, as well as to show the relation between elastic constants and its geometry parameters.

In this work, anti-tetrachiral anisotropic lattices have been manufactured using rapid prototype (RP)-based techniques, and subjected to in-plane tensile, flatwise compression and 3-point bending tests. Analytical models to describe the elastic constants of anisotropic anti-tetrachiral honeycomb configurations have been developed, and benchmarked against finite element (FE) homogenization methods and the experimental results. The validated analytical and numerical models have then used to perform a parametric analysis about the dependency of the linear elastic constant vs. the different honeycomb geometry parameters.

2. Anti-tetrachiral geometry and models for the linear elastic behavior

2.1. Lattice geometry

Fig. 1 shows a representative unit cell of the anti-tetrachiral anisotropic honeycomb configuration. The parameters L_x, L_y, r, and t represent the ligament length along the x and y directions, the radius of the node, and the wall thickness of the ligaments and nodes, respectively. The depth of the cell b is not shown for clarity. For convenience, four non-dimensional parameters are defined: $\alpha_x = L_x/r$, $\alpha_y = L_y/r$, $\beta = t/r$, $\gamma = b/r$.

2.2. Analytical formulation

As a first approximation, Prall and Lakes (1996) and Alderson et al. (2010a) assume that the nodes in structural chiral configurations are perfectly rigid rotating units, and only small deformations occur within the ligaments. The in-plane Young's modulus and Poisson's ratio can be derived for anti-tetrachiral isotropic honeycomb making use of conventional beam theory associated to the deformation mechanism of the ligaments. For the anisotropic (or special orthotropic) anti-tetrachiral configuration, we consider one ligament subjected to an axial load causing the attached node to rotate, and inducing also other adjacent nodes to rotate and ligaments to bend (Abramovitch et al., 2010). When the node rotates by an angle ϕ, the strains along the x (ε_x) and y (ε_y) directions can be expressed as (Fig. 2(a)):

$$\varepsilon_x = \frac{2(r - t/2)\phi}{L_x} \tag{1}$$

$$\varepsilon_y = \frac{2(r - t/2)\phi}{L_y} \tag{2}$$

The in-plane Poisson's ratio v_{xy} can be calculated from its definition (Evans and Alderson, 2000b):

$$v_{xy} = -\frac{\varepsilon_y}{\varepsilon_x} = -\frac{L_x}{L_y} \tag{3}$$

The energy approach is used here to obtain the in-plane linear elastic modulus. It is assumed that the strain energy generated by a small strain ε_i along the i direction is equated to the energy W_{lig} stored in each of the eight bent ligaments of the representative unit cell:

$$\frac{1}{2}E_i\varepsilon_i^2 = \frac{8}{V}W_{lig} \tag{4}$$

where E_i and V ($V = 4L_xL_yb$) are the elastic modulus in i direction and volume of the representative unit cell respectively. It is worth pointing out that the neutral axis of the ligament does not coincide with the outer surface of the node. From Fig. 1, the effective flexural length along the x and y directions (L_{ex} and L_{ey}) could be expressed as:

$$L_{ex} = L_x - 2\sqrt{r^2 - (r-t)^2} = L_x - 2\sqrt{2rt - t^2} \tag{5}$$

$$L_{ey} = L_y - 2\sqrt{r^2 - (r-t)^2} = L_y - 2\sqrt{2rt - t^2} \tag{6}$$

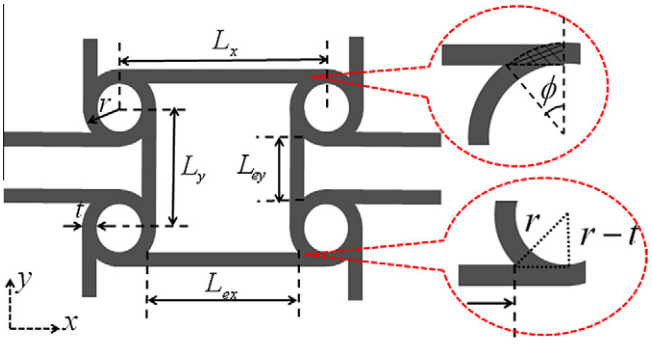

Fig. 1. Geometry of the anti-tetrachiral anisotropic honeycomb unit cell.

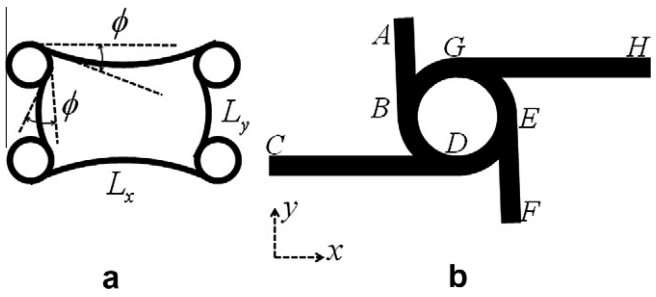

Fig. 2. Anti-tetrachiral anisotropic topology and simplified deformation: (a) the bending deformation of the lattice structure; (b) geometry definition for 1/4th of unit cell.

According to Euler–Bernoulli beam theory, two equal and opposing moments M acting on each end of the ligament produce a angular deflection ϕ. The strain energy of the beams can be therefore expressed as:

$$W_{lig} = 2\int_0^{\phi} M d\phi \tag{7}$$

For a ligament with effective flexural length L_{eff} and rectangular cross-section, the second moment of inertia is:

$$\phi = \frac{ML_{eff}}{2E_c I}, \quad I = \frac{bt^3}{12} \tag{8}$$

where E_c is the elastic modulus of core material. Substituting Eq. (8) into Eq. (7), a new expression for W_{lig} can be obtained:

$$W_{lig} = \frac{E_c b t^3 \phi^2}{6L_{eff}} \tag{9}$$

When small strains ε_x and ε_y are applied to the representative unit cell, two new energy expressions can be obtained by substituting equations (1), (2), and (9) into Eq. (4):

$$\frac{1}{2}E_x\varepsilon_x^2 = 4\left[\frac{E_c b t^3 L_x^2 \varepsilon_x^2}{24L_{ex}(r-t/2)^2} + \frac{E_c b t^3 L_x^2 \varepsilon_x^2}{24L_{ey}(r-t/2)^2}\right]\frac{1}{4L_xL_yb} \tag{10}$$

$$\frac{1}{2}E_y\varepsilon_y^2 = 4\left[\frac{E_c b t^3 L_y^2 \varepsilon_y^2}{24L_{ex}(r-t/2)^2} + \frac{E_c b t^3 L_y^2 \varepsilon_y^2}{24L_{ey}(r-t/2)^2}\right]\frac{1}{4L_xL_yb} \tag{11}$$

where E_x and E_y are the elastic moduli along the x and y directions of anti-tetrachiral anisotropic lattice. Eqs. (10) and (11) can be re-written in terms of non-dimensional geometry parameters as:

$$E_x = \frac{E_c\beta^3\alpha_x}{12\left(1-\frac{\beta}{2}\right)^2\alpha_y}\left(\frac{1}{\alpha_x - 2\sqrt{2\beta-\beta^2}} + \frac{1}{\alpha_y - 2\sqrt{2\beta-\beta^2}}\right) \tag{12}$$

$$E_y = \frac{E_c\beta^3\alpha_y}{12\left(1-\frac{\beta}{2}\right)^2\alpha_x}\left(\frac{1}{\alpha_x - 2\sqrt{2\beta-\beta^2}} + \frac{1}{\alpha_y - 2\sqrt{2\beta-\beta^2}}\right) \tag{13}$$

When ligament lengths are equal (i.e. $\alpha_x = \alpha_y = \alpha$), we obtains the expression for the in-plane Young's modulus related to isotropic anti-tetrachiral honeycombs (Alderson et al., 2010a):

$$E_x = E_y = \frac{E_c\beta^3}{6\left(1-\frac{\beta}{2}\right)^2}\left(\frac{1}{\alpha - 2\sqrt{2\beta-\beta^2}}\right) \tag{14}$$

Since the cellular structures are assumed to have a uniform wall thickness and depth for both nodes and ligaments, the elastic modulus E_z along the z direction can is proportional to the relative density of the honeycomb structure itself (Gibson and Ashby, 1997):

$$\frac{E_z}{E_c} = \frac{\rho}{\rho_c} \tag{15}$$

where ρ_c and ρ are the density of the core material and lattice structure respectively. By inspection, the relative density of the representative unit cell can be simplified as the ratio between core material area (A_c) and unit cell area (A_u) (Lorato et al., 2010):

$$\frac{\rho}{\rho_c} = \frac{A_c}{A_u} = \frac{A_n + A_l - A_j}{A_u} \tag{16}$$

where A_n, A_l and A_j are respectively the nodes, ligaments and junction areas of each unit cell. The junction area is represented by the overlap region between ligament and node (Fig. 1). The elastic modulus along the z direction can be therefore expressed as:

$$E_z = \frac{\beta[\alpha_x + \alpha_y + \pi(2-\beta)] - 2[\phi - (1-\beta)\sin\phi]}{\alpha_x\alpha_y}E_c \tag{17}$$

where $\phi = \arccos(1-\beta)$. Similarly, when the ligament lengths are equal, one obtains the expression for the anti-tetrachiral isotropic honeycomb (Lorato et al., 2010):

$$E_z = \frac{\beta[2\alpha + \pi(2-\beta)] - 2[\phi - (1-\beta)\sin\phi]}{\alpha^2}E_c \tag{18}$$

From a theoretical point of view, the transverse shear modulus of general honeycomb structures is limited within an upper (Voigt) and a lower (Reuss) bound. Those bounds can be obtained using the theorems of minimum potential energy and minimum complementary energy (Gibson and Ashby, 1997; Kelsey et al., 1958; Lira et al., 2009; Xu et al., 2001). For isotropic regular hexagonal lattices, the upper bound does coincide with the lower bound (Olympio and Gandhi, 2010). Although anti-tetrachiral isotropic honeycombs are in-plane isotropic, two different bounds for the transverse shear modulus exist (Lorato et al., 2010). In the present work, the upper limit of the transverse shear modulus is calculated using the theorem of minimum potential energy, which states that the potential energy is a minimum for compatible displacements (Olympio and Gandhi, 2010). Due to the in-plane symmetry of the anti-tetrachiral anisotropic lattice, a 1/4th unit cell is used for the analytical derivation (Fig. 2(b)). If a global transverse shear strain γ_{xz} is applied to the quarter unit cell, one obtains the following expression for the potential energies of the system (Gibson and Ashby, 1997):

$$\frac{1}{2}G_{xz}\gamma_{xz}^2 V_{1/4} \leqslant \frac{1}{2}G_c\sum_i(\gamma_i^2 V_i) \tag{19}$$

where G_{xz} and $V_{1/4}$ ($V_{1/4} = bL_xL_y$) are the transverse shear modulus of the anti-tetrachiral honeycomb and the volume of the quarter unit cell respectively. The symbols G_c, γ_i and V_i stand for the shear modulus of the core material, the transverse shear strain and volume components of the quarter unit cell. The shear strain and energy in each component of the 1/4th cell can be approximated by:

$$\gamma_i^{AB} = \gamma_i^{EF} = 0, \quad (\gamma_i^2 V_i)^{AB} = (\gamma_i^2 V_i)^{EF} = 0 \tag{20}$$

$$\gamma_i^{CD} = \gamma_i^{GH} = \gamma_{xz}, \quad (\gamma_i^2 V_i)^{CD} = (\gamma_i^2 V_i)^{GH} = \frac{L_x}{2}\gamma_{xz}^2 \tag{21}$$

$$(\gamma_i^2 V_i)^{node} = \int_0^{2\pi} rtb\gamma_{xz}^2 \sin\theta d\theta = \gamma_{xz}^2 \pi rtb \tag{22}$$

Substituting Eqs. (18)–(20) into Eq. (17), the upper bound of transverse shear modulus can be expressed in terms of the core shear modulus G_c and the nondimensional parameters as:

$$G_{xz} \leqslant \frac{(\alpha_x + \pi)}{\alpha_x\alpha_y}\beta G_c \tag{23}$$

Similarly, the upper bound of transverse shear modulus G_{yz} can be written in the following manner:

$$G_{yz} \leqslant \frac{(\alpha_y + \pi)}{\alpha_x\alpha_y}\beta G_c \tag{24}$$

Equal ligament lengths lead to the isotropic anti-tetrachiral formulation (Lorato et al., 2010):

$$G_{xz} = G_{yz} \leqslant \frac{(\alpha + \pi)}{\alpha^2}\beta G_c \tag{25}$$

Following Lorato et al. (2010), the lower bound is derived using a FEM approach with an estimation possible to each when considering honeycomb configurations with depth ratio γ around 20, because

the transverse shear modulus keeps almost constant for $\gamma > 17$ for a given set of wall aspect ratios and relative density values (Lorato et al., 2010). In this work, the lower bound for the transverse shear modulus of the anisotropic anti-tetrachiral lattices is identified for a depth ratio of 21. A non-linear least square (NLLS) fitting over 140 configurations of anti-tetrachiral anisotropic honeycomb provides the estimation of the actual transverse shear modulus:

$$G = G_{low} + K(G_{up} - G_{low}) \tag{26}$$

where G_{up} and G_{low} are the upper bound and lower bound of transverse shear modulus, respectively. The coefficient K ($R^2 = 0.9991$) can be written as:

$$K = 1 - 0.136\gamma + 0.00679\gamma^2 - 0.0001237\gamma^3 \quad (0 < \gamma \leqslant 21) \tag{27}$$

Eq. (27) is a higher polynomial order approximation of the dependency of the transverse shear vs. the depth ratio, compared to the simple inverse proportion existing in isotropic chiral configurations (Lorato et al., 2010), and centresymmetric hexagonal honeycomb layouts (Grediac, 1993; Scarpa and Tomlin, 2000).

2.3. FE Homogenization

In order to obtain the in-plane and out-of-plane linear elastic constants of the honeycomb structures, numerical homogenization procedures related to periodic continuum media (Odegard, 2004; Sun and Vaidya, 1996) have been performed using a commercial FE analysis package (ANSYS, version 11.0, Ansys Inc.). The models have been developed using 3D structural solid hexahedral elements SOLID45 with eight nodes and three translational degrees of freedom (nodal x, y and z directions). The element can also incorporate orthotropic core materials properties with the material axis corresponding to the element coordinate system. Convergence tests have determined a typical representative FE volume given by 4×4 cells and elements with minimum size of $t/2$ (Fig. 3).

The boundary conditions have been applied following (Odegard, 2004) (Table 1). The symbols u_x, u_y and u_z stand for the applied displacements along the x, y and z directions, respectively. The uniform axial strain and shear strain applied to the representative unit cell are expressed as ε_0 and γ_0 respectively. The coordinates of the element nodes are represented by x_i ($i = 1, 2,$ and 3), i.e. x, y and z directions. For example, loading along the x direction is performed with x-displacements (u_x) applied to the element nodes on both right-hand and left-hand surfaces (A and B), which are perpendicular to x-coordinate axis. The displacements are proportional to the uniform axial strain ε_0. The element nodes on both surfaces are also constrained from displacement along the y and z directions, while the element nodes on other four areas (C, D, E and F) are free. Strain along the $i = (x, y$ and $z)$ direction ($\bar{\varepsilon}_x$, $\bar{\varepsilon}_y$ and $\bar{\varepsilon}_z$) are calculated dividing the average displacement along the i direction by the original length of the lattice model. Average stresses along the $i = (x, y$ and $z)$ direction are calculated using the following formulation (Sun and Vaidya, 1996):

$$\bar{\sigma}_{xx} = \frac{1}{V}\int_V \sigma_{ii}(x, y, z)dV \tag{28}$$

According to Eq. (28) and the stress–strain relation expressed in (29), it is possible to calculate the homogenized stress–strain coefficients S_{11}, S_{21} and S_{31} for the periodic equivalent continuum medium representing the anti-tetrachiral configurations:

$$\begin{Bmatrix} \bar{\varepsilon}_x \\ \bar{\varepsilon}_y \\ \bar{\varepsilon}_z \\ \bar{\gamma}_{yz} \\ \bar{\gamma}_{zx} \\ \bar{\gamma}_{xy} \end{Bmatrix} = \begin{bmatrix} S_{11} & S_{12} & S_{13} & 0 & 0 & 0 \\ S_{21} & S_{22} & S_{23} & 0 & 0 & 0 \\ S_{31} & S_{32} & S_{33} & 0 & 0 & 0 \\ 0 & 0 & 0 & S_{44} & 0 & 0 \\ 0 & 0 & 0 & 0 & S_{55} & 0 \\ 0 & 0 & 0 & 0 & 0 & S_{66} \end{bmatrix} \begin{Bmatrix} \bar{\sigma}_x \\ \bar{\sigma}_y \\ \bar{\sigma}_z \\ \bar{\tau}_{yz} \\ \bar{\tau}_{zx} \\ \bar{\tau}_{xy} \end{Bmatrix} \tag{29}$$

$$\bar{\sigma}_x = \bar{\sigma}_{xx} - v_c(\bar{\sigma}_{yy} + \bar{\sigma}_{zz}) \quad (\bar{\sigma}_y = \bar{\sigma}_z = \bar{\tau}_{yz} = \bar{\tau}_{zx} = \bar{\tau}_{xy} = 0) \tag{30}$$

$$S_{11} = \bar{\varepsilon}_x/\bar{\sigma}_x, \quad S_{21} = \bar{\varepsilon}_y/\bar{\sigma}_x, \quad S_{31} = \bar{\varepsilon}_z/\bar{\sigma}_x \tag{31}$$

where v_c is the Poisson's ratio of the core material. Following a similar approach for the other homogenized stress–strain coefficients, it is possible to obtain the global second-order compliance homogenized tensor $[S]$. The in-plane and out-of-plane elastic constants of the honeycomb structures can be calculated from the elements of the compliance matrix as:

$$E_x = \frac{1}{S_{11}}, \quad E_y = \frac{1}{S_{22}}, \quad v_{xy} = -\frac{S_{21}}{S_{11}} \quad (\text{with } v_{xy}E_y = v_{yx}E_x)$$

$$E_z = \frac{1}{S_{33}}, \quad G_{yz} = \frac{1}{S_{44}}, \quad G_{xz} = \frac{1}{S_{55}} \tag{32}$$

There are nine elastic constants for the orthotropic anti-tetrachiral honeycomb. Since the terms E_x, E_y, E_z, G_{xz}, G_{yz} and v_{xy} are the primary concern of this current study, only the expressions of these six elastic constants are given.

3. Manufacturing and experimental testing

Anti-tetrachiral anisotropic honeycomb samples have been manufactured using a Rapid Prototyping (PR) Fusion Deposition Molding (FDM) Stratasys machine (Stratasys Inc., USA). The elastic properties of the core material (ABS plastic) have been determined from dog-bone specimens according to standard test method (ASTM D638-08) by some of the authors (Lira et al., 2011). Since the ABS plastic shows in-plane orthotropic mechanical properties ($E_x = 2016$ MPa, $v_{xy} = 0.43$; $E_y = 1530$ MPa, $v_{yx} = 0.41$), equivalent

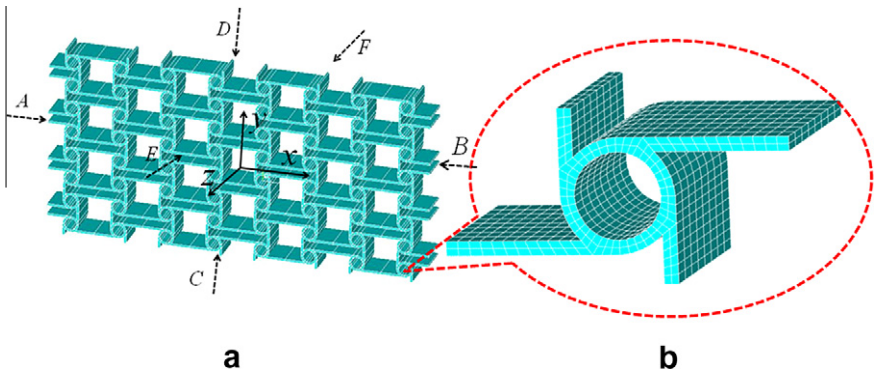

Fig. 3. Finite element model of repeating unit cell layout.

Table 1
Boundary conditions for the compliance matrix constants.

Properties	Element nodes displacement on surfaces A and B	Element nodes displacement on surfaces C and D	Element nodes displacement on surfaces E and F
$S_{i1}(i=1,2,3)$	$u_x = \varepsilon_0 x_1$ $u_y = 0$ $u_z = 0$	Free	Free
$S_{i2}(i=1,2,3)$	Free	$u_x = 0$ $u_y = \varepsilon_0 x_2$ $u_z = 0$	Free
$S_{i3}(i=1,2,3)$	Free	Free	$u_x = 0$ $u_y = 0$ $u_z = \varepsilon_0 x_3$
S_{44}	$u_x = 0$ $u_y = (\gamma_0/2)x_3$ $u_z = (\gamma_0/2)x_2$	$u_x = 0$ $u_y = (\gamma_0/2)x_3$ $u_z = (\gamma_0/2)x_2$	$u_x = 0$ $u_y = (\gamma_0/2)x_3$ $u_z = (\gamma_0/2)x_2$
S_{55}	$u_x = (\gamma_0/2)x_3$ $u_y = 0$ $u_z = (\gamma_0/2)x_1$	$u_x = (\gamma_0/2)x_3$ $u_y = 0$ $u_z = (\gamma_0/2)x_1$	$u_x = (\gamma_0/2)x_3$ $u_y = 0$ $u_z = (\gamma_0/2)x_1$
S_{66}	$u_x = (\gamma_0/2)x_2$ $u_y = (\gamma_0/2)x_1$ $u_z = 0$	$u_x = (\gamma_0/2)x_2$ $u_y = (\gamma_0/2)x_1$ $u_z = 0$	$u_x = (\gamma_0/2)x_2$ $u_y = (\gamma_0/2)x_1$ $u_z = 0$

isotropic properties ($E_c = 1756$ MPa, $v_c = 0.42$ and $G_c = 618.3$ MPa) are obtained using the geometric mean for the orthotropic elastic modulus and Poisson's ratio (Lira and Scarpa, 2010). For convenience, the equivalent isotropic elastic constants will be used in the FEM homogenization and theoretical formulas.

The elastic modulus of the anti-tetrachiral lattices along the z direction has been obtained from the flatwise compressive tests performed according to the ASTM standard C365/C365M-11a. The honeycomb samples (dimensions of 96 mm × 96 mm × 16 mm) have been tested on a tensile machine (Instron DX600) with a 600 KN load cell (Fig. 4(a)). A constant displacement rate of 0.5 mm/min has been used during the test. The force and displacement values have been recorded by a BlueHill control and acquisition software. In order to improve the test accuracy, a video extensometer has been used to record the accurate strain and displacement value. This system consists a digital video camera (SONY XCD-X710) with zoom lens (COMPUTAR 18-108/2.5) connected to a PC with video Gauge software (IMETRUM Ltd.) able to track and measure the position in pixels of targets marked on the sample during the test. In order to obtain the actual displacement, a reference displacement was used to convert the pixels into actual metric values (Thill et al., October 6–9, 2008). All the in-plane tensile tests were performed using a testing machine (Instron 3343, load cell: 1 KN) with a constant displacement rate of 1 mm/min. The honeycomb samples had dimensions of 192 mm × 96 mm × 2 mm for the tests related to the elastic modulus along both the x and y directions (Fig. 4(c) and (d)). A pair of custom clamps for the test were designed and manufactured, since the length of the honeycomb sample edge is larger the one of the machine jaw. These clamps are highlighted on Fig. 4(c) and (d). The sample strains along the x and y directions (ε_x and ε_y) could be obtained by measuring the positions of any two targets along the x and y directions, respectively. Base on the measurement results, the in-plane Poisson's ratio could be obtained using Eq. (3). The three-point bending tests have been performed using a testing machine (Zwick 1478, load cell: 100 KN) with a constant displacement rate of 0.5 mm/min (Fig. 4(b)). The honeycomb samples manufactured for the transverse shear modulus G_{xz} had dimensions 192 mm × 48 mm × 16 mm, 96 mm × 48 mm × 16 mm for the specimens made to measure G_{yz}. The face skins were produced using four layers of unidirectional prepreg IM7/8552 (Hexcel Corporation), with ply angles of $(+45/-45)_2$. After been surface treated with sandpaper, the face skins have a resultant thickness of 0.4 mm for the sandwich sample related to the G_{xz} measurement, and 0.3 mm for the G_{yz} sandwich beam. Two face skins have been bonded to the top and bottom surfaces of the honeycomb with a 2-part paste epoxy (REDUX 810, Hexcel Corporation) for a cold curing of 72 h. The final sandwich structure can also be found in Fig. 4(b). The transverse shear modulus of the sandwich beams has been calculated through the expression (Allen, 1969; Lira et al., 2011):

$$\Delta = \frac{WL^3}{48D} + \frac{WL}{4AG} \tag{33}$$

where G, Δ and W are respectively the transverse shear modulus, central deflection and central point load. L, D and A represent the length, flexural rigidity and cross-sectional area of the sandwich structures respectively.

4. Results and discussions

4.1. Comparison between experiments and models

The geometrical parameters of the anti-tetrachiral anisotropic honeycomb samples for the experimental tests related to the out-of-plane elastic constants are r=4 mm, L_x=24 mm, L_y=12 mm, t=1 mm and b=16 mm (i.e. $\alpha_x = 6$, $\alpha_y = 3$, $\beta = 0.25$ and $\gamma = 4$). Since the depth b is independent of the in-plane elastic modulus and in-plane Poisson's ratio, b=2 mm has been chosen for the specimen to be tested to identify the in-plane elastic mechanical properties. Table 2 shows the comparison of the elastic constants between the theory, FE homogenization and the experimental results. The FE results show a discrepancy of 6.9% and 9.2% over the experimental results related to E_z and G_{xz}, and 19.5% for G_{yz}. The in-plane elastic constants E_x and E_y show a 2.17% and 9.5% difference with the experimental findings. Uncertainties affecting the discrepancy between the experimental and analytical and FE results can be ascribed also to the use of an equivalent isotropic elastic modulus E_c (=1756 MPa). The samples produced using FDM techniques have a layerwise deposition of the ABS plastics, and a degree of internal porosity that is not consistent with the assumption of an isotropic and homogeneous core material for these lattice structures (Bellini and Güçeri, 2003; Lira and Scarpa, 2010; Lira et al., 2011). There is however a general excellent agreement between the theoretical and FE homogenization models, with a discrepancy lower than 2.7% for E_y, E_z, G_{xz} and G_{yz}, as well as a discrepancy of 8.7% and 7.5% for the elastic modulus E_x and Poisson's ratio v_{xy} respectively.

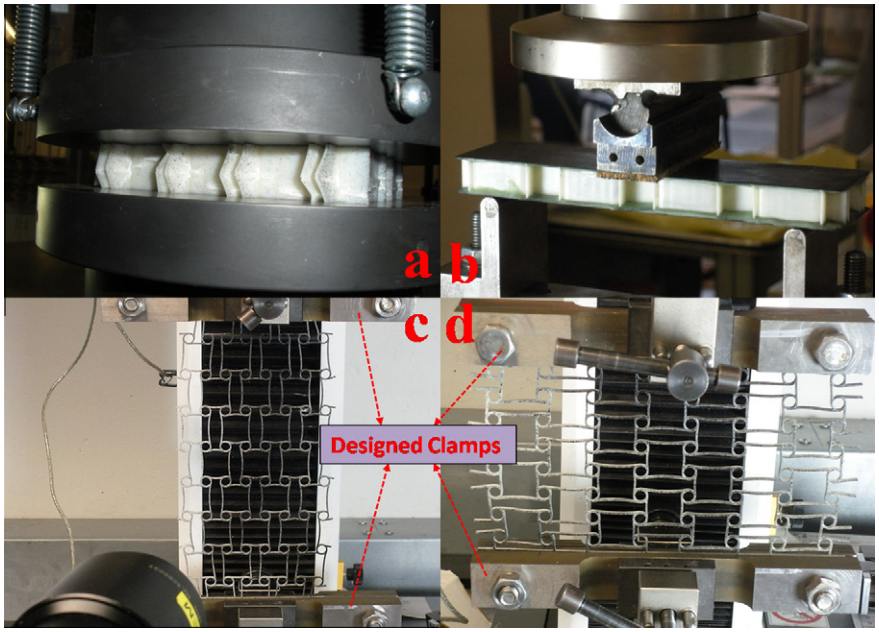

Fig. 4. Honeycomb structures experimental setup: (a) flatwise compression tests; (b) three-point bending tests; (c) and (d) tensile tests.

Table 2
Comparison between the theory, FEM and experimental results.

	Theory	FEM	Experiment
E_x (MPa)	4.838	5.260	5.374 ± 0.015
E_y (MPa)	1.209	1.242	1.360 ± 0.017
E_z (MPa)	309.4	308.8	280.5 ± 9.8
G_{xz} (MPa)	68.23	68.12	63.43 ± 2.92
G_{yz} (MPa)	42.62	42.86	34.65 ± 0.57
v_{xy}	−2.000	−1.849	−1.831 ± 0.005

4.2. Parametric analysis

4.2.1. Uniaxial stiffness constants

Figs. 5–7 shows the variation of the elastic properties of the anti-tetrachiral configurations vs. the geometry parameters of the unit cells. The curves are obtained via the analytical and FE homogenization models. Considering the in-plane symmetry of the anti-tetrachiral honeycomb and the special orthotropic relation

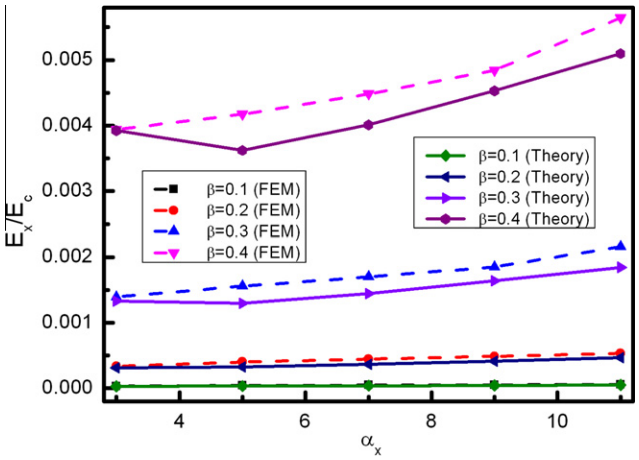

Fig. 6. FE homogenization and analytical predictions for the non-dimensional elastic modulus (E_x/E_c) vs. α_x ($=L_x/r$) for different β ($=b/r$).

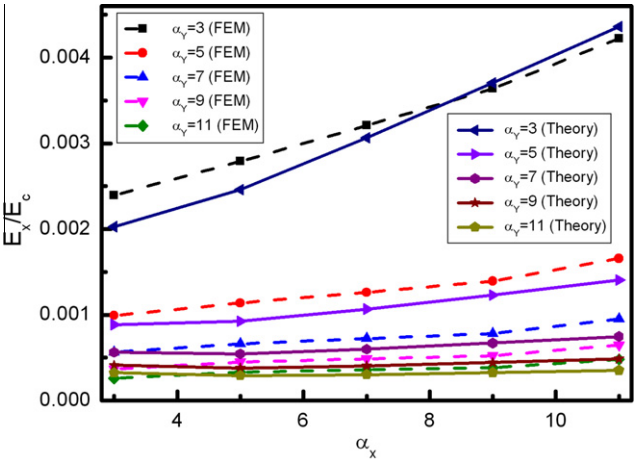

Fig. 5. FE homogenization and analytical predictions for the non-dimensional elastic modulus (E_x/E_c) vs. α_x ($=L_x/r$) for different α_y ($=L_y/r$).

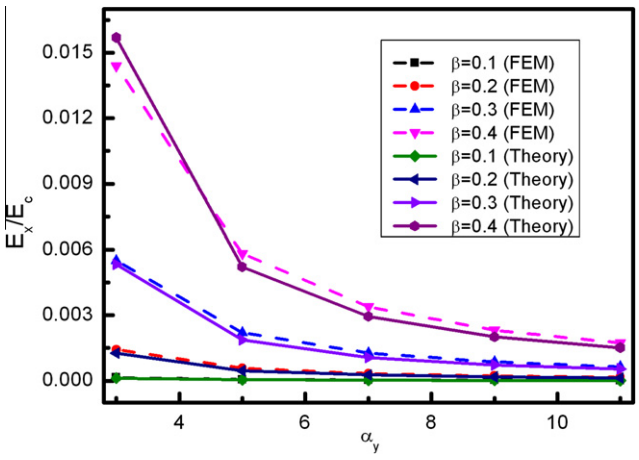

Fig. 7. FE homogenization and analytical predictions for the non-dimensional elastic modulus (E_x/E_c) vs. α_y ($=L_y/r$) for different β ($=b/r$).

($\nu_{xy}E_y = \nu_{yx}E_x$), only the elastic modulus E_x is analyzed and discussed in this section. Fig. 5 shows the predictions related to the non-dimensional elastic modulus (E_x/E_c) vs. α_x for different α_y values (with $r = 4$ mm, $\gamma = 4$ and $\beta = 0.25$). It is worth to notice that the FE values show a stiffer response (average value: 10.97%) compared to the analytical results. The FE nodes present on the two surfaces A and B have been constrained from displacement along the y and z directions (u_y and u_z) and, in that sense, are more representative of the experimental tensile boundary conditions. The end effect generated by this constraint is not present in the theoretical model. In general, the non-dimensional elastic modulus (E_x/E_c) increases with increasing α_x values for α_y constant. On the opposite, the non-dimensional elastic modulus (E_x/E_c) decreases for increasing α_y values, while α_x is kept as constant parameter (Fig. 5).

The FE and analytical models related to the non-dimensional elastic modulus vs. α_x (with $r = 4$ mm, $\gamma = 4$ and $\alpha_y = 6$) and α_y (with $r = 4$ mm, $\gamma = 4$ and $\alpha_x = 6$) for different β values are shown in Figs. 6 and 7 respectively. The ratio E_x/E_c increases for increasing α_x when β is kept constant, but the opposite is true for increasing α_y values, for which it is possible to observe a decrease of the non-dimensional Young's modulus (Fig. 7). For higher non-dimensional wall thickness (β), E_x/E_c exhibits in both figures a non-linear increase when the non-dimensional ligament lengths α_x and α_y remain constant. The phenomenon can be explained observing Eq. (12), which contains a β^3 term in the numerator, in similarity with what is observed also for in-plane stiffness properties centre-symmetric honeycombs (Gibson and Ashby, 1997).

Fig. 8 shows the behavior of E_z/E_c vs. α_x for different α_y (with $r = 4$ mm, $\gamma = 4$ and $\beta = 0.25$) values. When α_y is kept constant, the non-dimensional transverse elastic modulus decreases with increasing values of α_x, reaching its minimum value (β/α_y) when α_x is infinitely large. Similarly, when α_x is kept constant, E_z/E_c decreases with increasing values of α_y. The non-dimensional transverse elastic modulus will reach its minimum value (β/α_x) when α_y tends towards infinity. The explanation for this trend can be found observing Eq. (17), in which the non-dimensional parameter α_x and α_y give an equal contribution to the behavior of E_z. Therefore, only α_x is used to study the effect of the geometry on the transverse elastic modulus E_z in the following discussions. Fig. 9 shows the behavior of the transverse non-dimensional elastic modulus E_z/E_c vs. α_x for different β (with $r = 4$ mm, $\gamma = 4$ and $\alpha_y = 6$) values. When β is kept constant, the non-dimensional elastic modulus (E_z/E_c) decreases with increasing α_x values. However, when α_x is made constant, the non-dimensional transverse elastic modulus increases for increasing β. An excellent agreement between the FE homogenization and theoretical values can be observed.

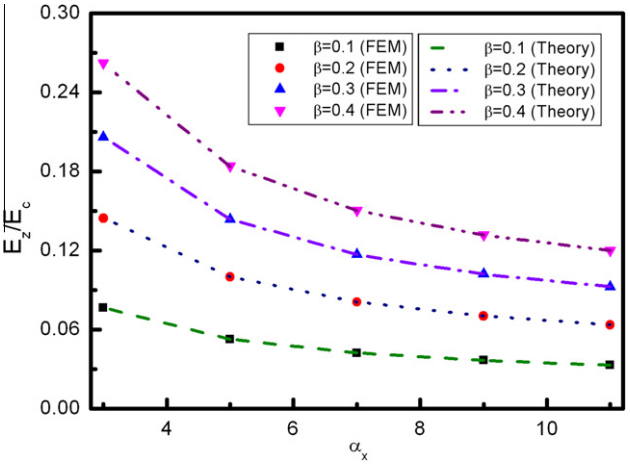

Fig. 9. FE homogenization and analytical predictions for the non-dimensional transverse elastic modulus (E_z/E_c) vs. α_x (=L_x/r) for different β (=b/r).

4.2.2. Poisson's ratios

Fig. 10 shows the comparison between FE homogenization and analytical results for the in-plane Poisson's ratio ν_{xy} vs. α_x for different α_y (with $r = 4$ mm, $\gamma = 4$ and $\beta = 0.25$) values. In general, it is possible to observe a reasonable agreement between the numerical and theoretical values. The magnitude of the Poisson's ratio from the FE simulations is lightly lower (average values: 7.85%) than the one predicted by the theoretical model, showing a stiffer mechanical response from the FE homogenization. When α_y is kept constant, the in-plane negative Poisson's ratio ν_{xy} increases with the increasing of α_x. On the opposite, when α_x remains constant, the in-plane negative Poisson's ratio ν_{xy} decrease for increasing α_y value, as expected by inspecting equation (3). The result indicates that large variations in in-plane negative Poisson's ratio can be achieved through changing the ligament lengths along the x and y directions.

4.2.3. Transverse shear moduli

The transverse shear modulus is an important parameter for the bending stiffness of sandwich beams and plates (Bitzer, 1997).

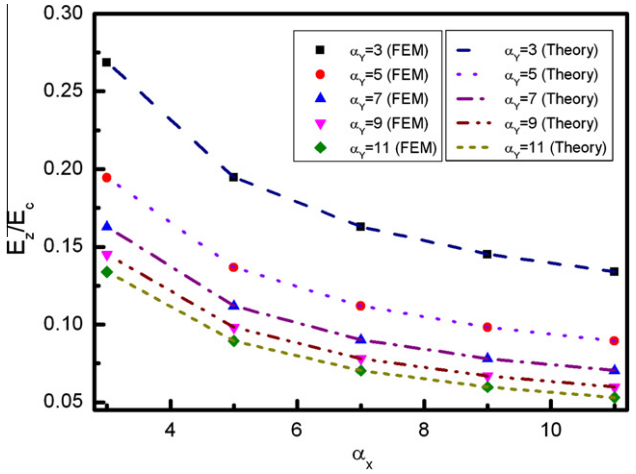

Fig. 8. FE homogenization and analytical predictions for the non-dimensional transverse elastic modulus (E_z/E_c) vs. α_x (=L_x/r) for different α_y (=L_y/r).

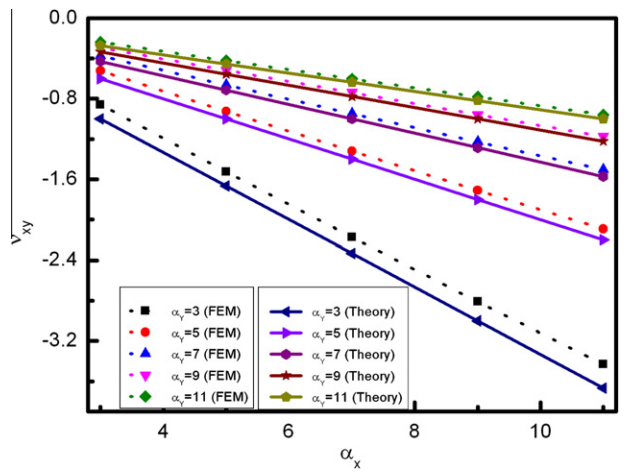

Fig. 10. FE homogenization and theoretical predictions related to the Poisson's ratio (ν_{xy}) vs. α_x (=L_x/r) for different α_y (=L_y/r).

Only transverse shear modulus G_{xz} is discussed in this section due to the symmetry properties of the anti-tetrachiral lattice configuration. Figs. 11–13 show the comparison between the FE homogenization and theoretical predictions of transverse shear modulus vs. different geometry parameters of the anti-tetrachiral unit cell. As seen in these figures, all the FE-derived results show a good agreement with the theoretical ones. The behavior of non-dimensional transverse shear modulus ($G_{xz}/(\beta G_c)$) vs. α_x for different α_y (with $r = 4$ mm, $\gamma = 4$ and $\beta = 0.25$) values is shown in Fig. 11. Along with increasing values of α_x, the non-dimensional transverse shear modulus decreases when α_y is kept constant. Similarly, for increasing α_y values, $G_{xz}/(\beta G_c)$ tends to decrease.

The variation of the non-dimensional transverse shear modulus ($G_{xz}/(\beta G_c)$) vs. the depth ratio γ for different α_x (with $r = 4$ mm, $\beta = 0.25$ and $\alpha_y = 6$) and α_y (with $r = 4$ mm, $\beta = 0.25$ and $\alpha_x = 6$) values are illustrated in Figs. 12 and 13 respectively, showing a general excellent agreement. The non-dimensional transverse shear modulus decreases with increasing values of γ when α_x and α_y are kept constant. The transverse shear modulus first decreases rapidly, then approaches to an asymptotic behavior, which coincides with the lower bound (Fig. 12). A similar trend can also be observed in Fig. 13. Within the values range of depth ratio γ ($0 < \gamma \leqslant 21$), the non-dimensional transverse shear moduli reach their maximum values around zero and decrease to their minimum values at 21.

4.2.4. Specific mechanical properties

Density is an important design parameter when selecting core materials in lightweight sandwich applications (Bitzer, 1997). Fig. 14 shows the FE homogenization predictions related to the non-dimensional elastic modulus (E_x/E_c) vs. relative density (ρ/ρ_c) for different α_y (with $r = 4$ mm, $\beta = 0.25$, $\gamma = 4$ and $\alpha_x = 3, 5, 7, 9$ and 11) and α_x (with $r = 4$ mm, $\beta = 02.5$, $\gamma = 4$ and $\alpha_x = 3, 5, 7, 9$ and 11) values. For increasing relative density, the non-dimensional elastic moduli tend to decrease when α_y is kept constant, on the opposite increasing when α_x remains constant. For constant relative density (ρ/ρ_c), E_x/E_c increases for increasing α_x, on the opposite increasing for lower values of α_y. The results suggest the possibility of using anisotropic anti-tetrachiral configurations to design honeycomb structures with minimum density and maximizing in-plane elastic modulus. Similarly, Fig. 15 shows the predictions from the FE homogenization method related to the non-dimensional transverse shear modulus (G_{xz}/G_c) vs. relative density (ρ/ρ_c) for different α_y (with $r = 4$ mm, $\beta = 0.25$, $\gamma = 4$ and $\alpha_x = 3, 5, 7, 9$ and 11 and α_x (with $r = 4$ mm, $\beta = 0.25$, $\gamma = 4$ and

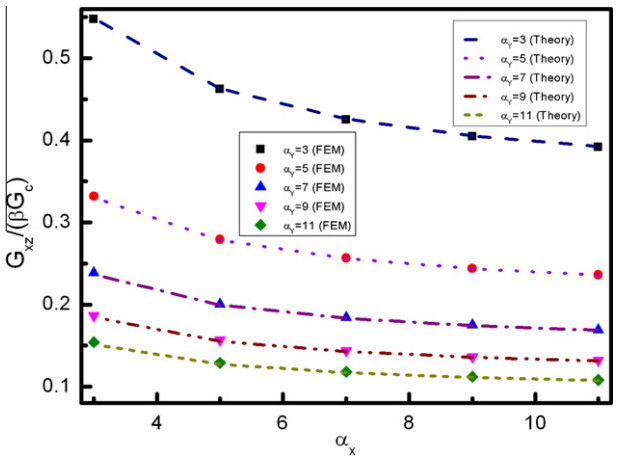

Fig. 11. FE homogenization and theoretical predictions for non-dimensional transverse shear modulus ($G_{xz}/(\beta G_c)$) vs. α_x ($=L_x/r$) for different α_y ($=L_y/r$).

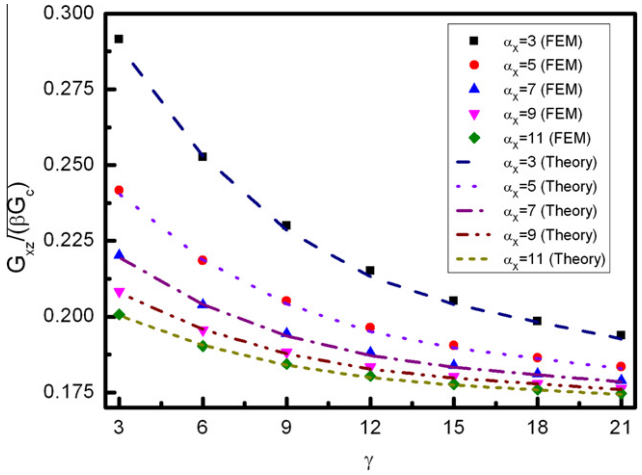

Fig. 12. FE homogenization and theoretical predictions related to the non-dimensional transverse shear modulus ($G_{xz}/(\beta G_c)$) vs. γ ($=t/r$) for different α_x ($=L_x/r$).

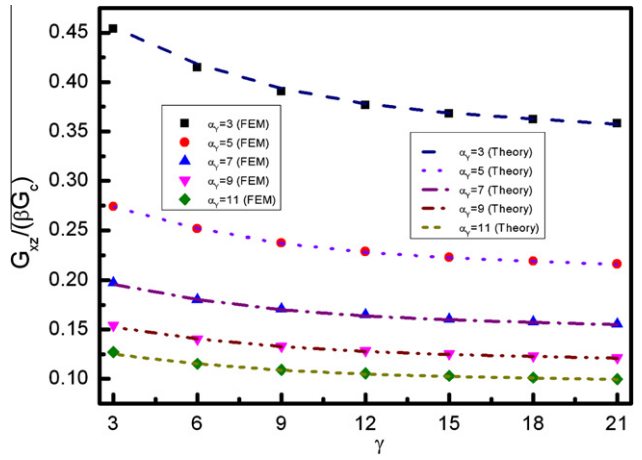

Fig. 13. FE homogenization and theoretical predictions for the non-dimensional transverse shear modulus ($G_{xz}/(\beta G_c)$) vs. γ ($=t/r$) for different α_y ($=L_y/r$).

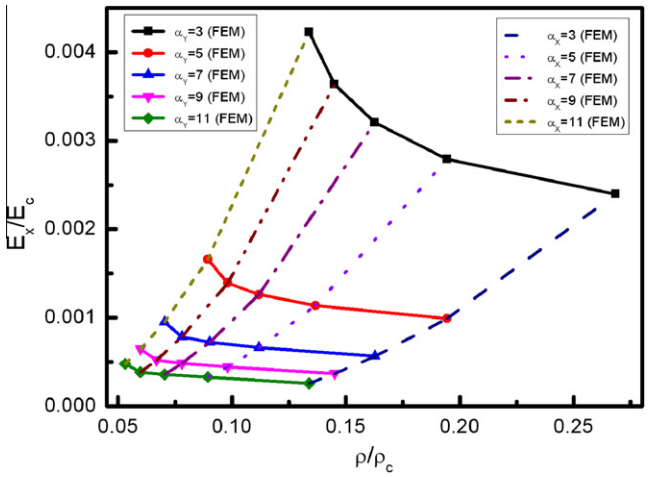

Fig. 14. FE homogenization predictions related to the non-dimensional elastic modulus (E_x/E_c) vs. relative density (ρ/ρ_c) for different α_y ($=L_y/r$) and different α_x ($=L_x/r$).

$\alpha_x = 3, 5, 7, 9$ and 11) values. For increasing relative density, the non-dimensional transverse shear moduli tend to increase when

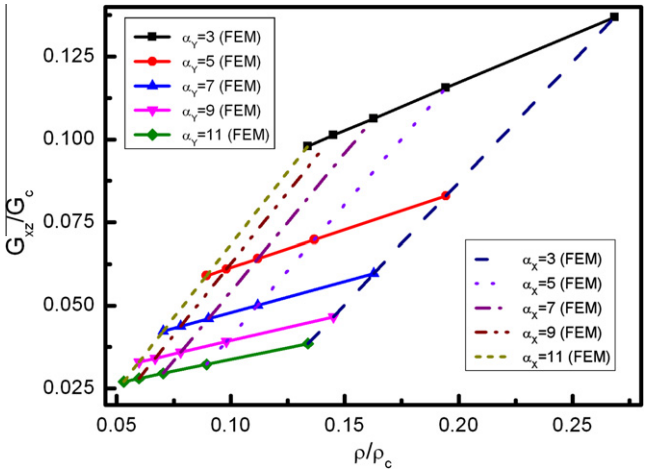

Fig. 15. FE homogenization predictions for the non-dimensional transverse shear modulus (G_{xz}/G_c) vs. relative density (ρ/ρ_c) for different α_y ($=L_y/r$) and different α_x ($=L_x/r$).

α_y and α_x remain constants. At constant relative density (ρ/ρ_c), G_{xz}/G_c increases for decreasing α_y, on the opposite it diminishes its value for higher α_x parameters. Also these results indicate that it could be possible to design honeycomb structures with minimum density and maximum transverse shear modulus when using anisotropic anti-tetrachiral configurations.

5. Conclusions

In this work, a novel anti-tetrachiral anisotropic lattice structure has been modeled, produced with rapid prototyping techniques and investigated from an analytical, numerical and experimental point of view. The focus of the investigation was the effect of the anisotropic chiral lattice over the variation of the in-plane homogenized elastic uniaxial elastic constants (Young's moduli and Poisson's ratios), as well as the transverse shear moduli. The accuracy of theoretical and FE homogenization models has been validated by a series of experimental results carried out following standardized tests. A parametric analysis showed that one can expect large variations of the in-plane negative Poisson's ratios through changing the length of the ligaments along the x and y directions. Anti-tetrachiral anisotropic honeycomb structures with minimum density but maximum transverse shear modulus (or in-plane elastic modulus) can be identified through careful selection of the geometry parameters. The analysis presented in this work provides overall guidelines to develop and manufacture a new type of core for sandwich structures for a variety of engineering applications.

Acknowledgments

The Authors acknowledge the partial support of the European Project FP7-NMP-2009-LARGE-3M-RECT for the logistics of the manufacturing and experimental rigs. YJC would also like to thank CSC (Chinese Scholarship Council) for funding of his research work through the University of Bristol. Special thanks go also to the University of Bristol and Harbin Institute of Technology.

References

Abramovitch, H., Burgard, M., Edery-Azulay, L., Evans, K., Hoffmeister, M., Miller, W., Scarpa, F., Smith, C., Tee, K.F., 2010. Smart tetrachiral and hexachiral honeycomb: sensing and impact detection. Compos. Sci. Technol. 70, 1072–1079.

Alderson, A., Alderson, K., Attard, D., Evans, K., Gatt, R., Grima, J., Miller, W., Ravirala, N., Smith, C., Zied, K., 2010a. Elastic constants of 3-, 4-and 6-connected chiral and anti-chiral honeycombs subject to uniaxial in-plane loading. Compos. Sci. Technol. 70, 1042–1048.

Alderson, A., Alderson, K., Chirima, G., Ravirala, N., Zied, K., 2010b. The in-plane linear elastic constants and out-of-plane bending of 3-coordinated ligament and cylinder-ligament honeycombs. Compos. Sci. Technol. 70, 1034–1041.

Allen, H.G., 1969. Analysis and Design of Structural Sandwich Panels. Pergamon press, Oxford and New York.

Bellini, A., Güçeri, S., 2003. Mechanical characterization of parts fabricated using fused deposition modeling. Rapid Prototyping J. 9, 252–264.

Bettini, P., Airoldi, A., Sala, G., Landro, L.D., Ruzzene, M., Spadoni, A., 2010. Composite chiral structures for morphing airfoils: numerical analyses and development of a manufacturing process. Compos. B Eng. 41, 133–147.

Bezazi, A., Scarpa, F., Remillat, C., 2005. A novel centresymmetric honeycomb composite structure. Compos. Struct. 71, 356–364.

Bitzer, T., 1997. Honeycomb Technology: Materials, Design, Manufacturing, Applications and Testing. Chapman & Hall, London.

Evans, K., 1991. The design of doubly curved sandwich panels with honeycomb cores. Compos. Struct. 17, 95–111.

Evans, K., Alderson, K., 2000a. Auxetic materials: the positive side of being negative. Eng. Sci. Edu. J. 9, 148–154.

Evans, K.E., Alderson, A., 2000b. Auxetic materials: functional materials and structures from lateral thinking! Adv. Mater. 12, 617–628.

Gaspar, N., Ren, X., Smith, C.W., Grima, J., Evans, K.E., 2005. Novel honeycombs with auxetic behaviour. Acta Mater. 53, 2439–2445.

Gibson, L.J., Ashby, M.F., 1997. Cellular Solids: Structure and Properties, second ed. Cambridge University Press.

Grediac, M., 1993. A finite element study of the transverse shear in honeycomb cores. Int. J. Solids Struct. 30, 1777–1788.

Grima, J.N., 2000. New auxetic materials. Ph.D. Thesis, University of Exeter.

Hassan, M., Scarpa, F., Ruzzene, M., Mohammed, N., 2008. Smart shape memory alloy chiral honeycomb. Mater. Sci. Eng., A 481, 654–657.

Jenal, R., Staszewski, W., Scarpa, F., Tee, K.F., 2009. Damage detection in smart chiral sandwich structures using nonlinear acoustics. In: Proceedings of the 20th International Conference on Adaptive Structures and Technologies (ICAST), Hong Kong, China, October 20–22.

Kelsey, S., Gellatly, R., Clark, B., 1958. The shear modulus of foil honeycomb cores: a theoretical and experimental investigation on cores used in sandwich construction. Aircr. Eng. Aerosp. Technol. 30, 294–302.

Lakes, R., 1987. Foam structures with a negative Poisson's ratio. Science 235, 1038–1040.

Lira, C., Innocenti, P., Scarpa, F., 2009. Transverse elastic shear of auxetic multi re-entrant honeycombs. Compos. Struct. 90, 314–322.

Lira, C., Scarpa, F., 2010. Transverse shear stiffness of thickness gradient honeycombs. Compos. Sci. Technol. 70, 930–936.

Lira, C., Scarpa, F., Tai, Y., Yates, J., 2011. Transverse shear modulus of SILICOMB cellular structures. Compos. Sci. Technol. 71, 1236–1241.

Lorato, A., Innocenti, P., Scarpa, F., Alderson, A., Alderson, K., Zied, K., Ravirala, N., Miller, W., Smith, C., Evans, K., 2010. The transverse elastic properties of chiral honeycombs. Compos. Sci. Technol. 70, 1057–1063.

Martin, J., Heyder-Bruckner, J.J., Remillat, C., Scarpa, F., Potter, K., Ruzzene, M., 2008. The hexachiral prismatic wingbox concept. Phys. Status Solidi B 245, 570–577.

Masters, I., Evans, K., 1996. Models for the elastic deformation of honeycombs. Compos. Struct. 35, 403–422.

Miller, W., Smith, C., Scarpa, F., Evans, K., 2010. Flatwise buckling optimization of hexachiral and tetrachiral honeycombs. Compos. Sci. Technol. 70, 1049–1056.

Odegard, G.M., 2004. Constitutive modeling of piezoelectric polymer composites. Acta Mater. 52, 5315–5330.

Olympio, K.R., Gandhi, F., 2010. Flexible skins for morphing aircraft using cellular honeycomb cores. J. Intell. Mater. Syst. Struct. 21, 1719–1735.

Prall, D., Lakes, R., 1996. Properties of a chiral honeycomb with a Poisson's ratio of −1. Int. J. Mech. Sci. 39, 305–314.

Scarpa, F., Blain, S., Lew, T., Perrott, D., Ruzzene, M., Yates, J., 2007. Elastic buckling of hexagonal chiral cell honeycombs. Compos. A Appl. Sci. Manuf. 38, 280–289.

Scarpa, F., Smith, F.C., Chambers, B., Burriesci, G., 2003. Mechanical and electromagnetic behaviour of auxetic honeycomb structures. Aeronaut. J. 107, 175–183.

Scarpa, F., Tomlin, P., 2000. On the transverse shear modulus of negative Poisson's ratio honeycomb structures. Fatigue Fract. Eng. Mater. Struct. 23, 717–720.

Spadoni, A., Ruzzene, M., Scarpa, F., 2005. Global and local linear buckling behavior of a chiral cellular structure. Phys. Status Solidi 242, 695–709.

Spadoni, A., Ruzzene, M., Scarpa, F., 2006. Dynamic response of chiral truss-core assemblies. J. Intell. Mater. Syst. Struct. 17, 941–952.

Sun, C., Vaidya, R., 1996. Prediction of composite properties from a representative volume element. Compos. Sci. Technol. 56, 171–179.

Thill, C., Etches, J.A., Bond, I.P., Weaver, P.M., Potter, K.D., 2008. Experimental and parametric analysis of corrugated composite structures for morphing skin applications. In: Proceedings of the 19th International conference on Adaptive Structures and Technologise (ICAST), Ascona, Switzerland, October 6–9.

Xu, X.F., Qiao, P., Davalos, J.F., 2001. Transverse shear stiffness of composite honeycomb core with general configuration. J. Eng. Mech. 127, 1144–1151.